Journal of Materials Chemistry A

Accepted Manuscript

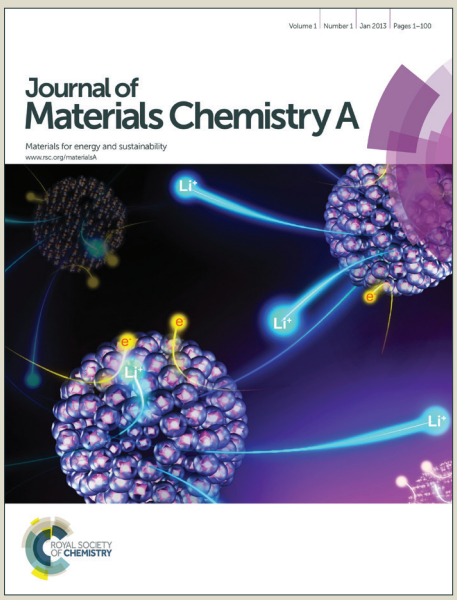

ROYAL SOCIETY OF CHEMISTRY

www.rsc.org/materialsA

ARTICLE TYPE www.rsc.org/xxxxxx | XXXXXXXX

Application in dye–sensitized solar cells and luminescence properties: an insight into the controllable synthesis of Cd(II) complexes with the new multifunctional ligand

Song Gao,[a] Rui Qing Fan,*[a] Xin Ming Wang,[a] Liang Sheng Qiang,[a] Li Guo Wei,[a] Ping Wang,[a] Hui Jie Zhang,[a] Yu Lin Yang*[a], Yu Lei Wang[b]

Received (in XXX, XXX) Xth XXXXXXXXX 200X, Accepted Xth XXXXXXXXX 200X
First published on the web Xth XXXXXXXXX 200X
DOI: 10.1039/b000000x

Based on a new design of 4-cyanobenzyl–based 1,2,4-triazole ligand 4-(1,2,4-triazolylmethyl) cyanobenzene (TMCB), a series cadmium complexes **1**–**5'** from mononuclear to three–dimensional (3D) structure have been synthesized through hydro(solvo)thermal reactions, generally formulated as $[Cd(TMCBA)_2]_n$ **(1)**, $[Cd(TMCB)(1,4\text{-bda})(H_2O)]_n$ **(2)**, $\{[Cd_2(TMCB)_4(1,4\text{-bda})_2(H_2O)_2]_n\cdot 3H_2O\}_n$ **(3)**, $\{[Cd(TMCB)_4(H_2O)_2]\cdot(NO_3)_2\cdot(H_2O)_2\}_n$ **(4)**, $[Cd_{1.5}(1,4\text{-bda})_{1.5}(DMF)_2]_{2n}$ **(5)** and $[Cd_{1.5}(1,4\text{-bda})_{1.5}(DMF)_2]_{2n}$ **(5')** (TMCBA = 4-(1,2,4-triazolylmethyl) benzoic acid, which is formed from the hydrolysis of TMCB; 1,4-H_2bda = 1,4-benzenedicarboxylic acid; the difference between two genuine supramolecular isomers of **5** and **5'** is to use TMCB as additive agent for the reaction). Complexes **1**–**5'** exhibit tunable luminescence with emission maxima containing deep blue, blue, light blue, green and deep green at 298 K or 77 K both in different solvents (polarity: DMSO > CH_3OH > $CHCl_3$) and in the solid state. Fascinatingly more, the good thermal stability accompanied by their compensated adsorption to ruthenium complex N719 in the region of low wavelength, enabled **1** and **4** serve as co-sensitizers in combination with N719 in dye sensitized solar cells (DSSCs), respectively. After co-sensitization with N719, the overall conversion efficiency of **1** and **4** can achieve 7.68% and 6.85%, which are 40.40% and 25.23% higher than that for DSSCs only sensitized by N719 (5.47%) under the same conditions, respectively. The improvement in efficiency is attributed to the fact that complexes **1** and **4** overcome the deficiency of N719 absorption in the low wavelength region of ultraviolet and blue-violet, offset competitive visible light absorption of I_3^- and reduce charge recombination due to formation of an effective cover layer of the dye molecules on the TiO_2 surface. As a result, the synthesized complexes are promising candidates as co-adsorbents and co-sensitizers for highly efficient DSSCs.

Introduction

The luminescent properties of metal coordination complexes (MCCs) have attracted ever growing attention in recent years.[1-4] These luminescence MCCs possess wider applications such as solvent sensor device,[5] smart windows,[6] ophthalmic lenses,[7] optical filters and optical memory,[8,9] *etc*. However, exploration of these luminescent behaviors is still a big challenge which could be influenced by complex thermal stability, photostability, solubility and other factors. The key to design luminescent materials is the matching of organic ligand and central metal ion which can provide the platforms to generate ultraviolet absorption and luminescence.[10-13]

As a typical representative of luminescent materials, Cd(II)-based MCCs have gained intensive attention mainly due to three aspects: (i) Cd(II) is lower-cost and easy to get for application. (ii) Cd(II) has a versatile mode of coordination (coordination number 4-8), which can lead to fascinating topological structures.[14] (iii) The presence of electronically saturated d^{10}-metal Cd(II) ion is appropriate because it imposes conformational rigidity to the ligand and prevents energy loss via bond vibration and electron transfer processes, whereas paramagnetic transition metals quench fluorescence by different electron/energy transfer mechanisms.[15] The enormous variability of available ligand–metal combinations opens the possibility of creating luminescence "by design". Up to now, complexes containing 1,2,4-triazole ligand and its derivatives have been widely studied in the construction of illuminant MCCs,[16-22] which have strong absorption in the ultraviolet and blue-violet region.[23,24] However, the 4-(1,2,4-triazolylmethyl)cyanobenzene (TMCB) (Scheme 1) and 4-(1,2,4-triazolylmethyl)benzoic acid (TMCBA) (through controlling the reaction conditions, TMCBA was produced from the cyanophoric hydrolytic reaction of TMCB) as representatively flexible ligands, are never investigated in this field. These flexible ligands TMCB

[a] *Department of Chemistry, Harbin Institute of Technology, Harbin, 150001 (P. R. China). E-mail: fanruiqing@hit.edu.cn (R. Q. Fan); ylyang@hit.edu.cn (Y. L. Yang)*
[b] *National Key Laboratory of Science and Technology on Tunable Laser, Harbin Institute of Technology, Harbin, 150025 (P. R. China)*

† Electronic supplementary information (ESI) available: Experimental details and results of luminescence experiments. The CIF files give crystallographic data for complexes **1**–**5'**. Fig. S1–S24, Scheme S1, Scheme S2 and Tables S1–S4. CCDC 1028900, 1028901, 1028902, 1028903, 1028904 and 1028905. For ESI and crystallographic data in CIF or other electronic format see DOI: 10.1039/b000000x

and TMCBA with π-conjugated system play crucial roles in determining the structure and luminescent properties of the complexes because of the diversiform coordination mode and the flexible nature of –CH_2– spacers.

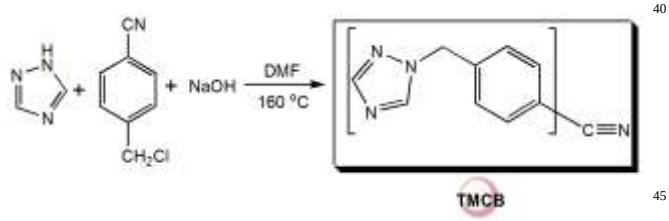

Scheme 1 Synthetic procedure of TMCB ligand.

As the rapid development of energy conversion devices, the MCCs with specific optical property are being applied in the dye sensitized solar cells (DSSCs) gradually.[25] In the photoelectric transformation, co-sensitization by means of multiple sensitizers including MCCs would appear to be more effective to improve the absorption ability of solar cell.[26] MCCs as co-sensitizer or co-adsorbent in DSSCs could not only compensate the absorption spectra but also overcome the competitive light absorption by I^-/I_3^-, avoid dye aggregation and reduce charge recombination, which will lead to enhanced DSSCs performance by co-sensitization.[27,28] Among numerous of MCCs, noble metal (Ir, Ru, Pd)[29-32] MCCs are introduced to DSSCs system as co-sensitizers. Although the noble metal MCCs show good photoelectric conversion performance, the expensive price hinders their practical application. The efforts for increasing solar cell efficiency with a low production cost have been the primary objective of solar energy conversion. For this reason, our group synthesized low-cost Cd(II) metal complexes, in order to replace precious metal complexes as co-sensitizers.

In this paper, the sensitive luminescence is realized by the rational design and controllable construction of six Cd(II) complexes from mononuclear to 3D network based on flexible ligand TMCB or TMCBA. Since the strong absorption in 320–378 nm and excellent stability, complexes **1** and **4** are selected to be co-sensitizers and applied in the DSSC system sensitized by N719, respectively. It is showed that the absorption spectra of complexes **1** and **4** could compensate for that of N719 in the low wavelength region of ultraviolet and blue-violet and the light harvesting was enhanced, which lead to 40.40% and 25.23% improvement of DSSCs performance than blank N719. Our research breaks through the low utilization problem of N719 absorption efficiency in ultraviolet and blue-violet region. Consequently, the excellent properties indicate the great potential of the MCCs being utilized as the multifunctional material in both luminescence and DSSCs fields.

Results and Discussion

Synthesis: We have successfully obtained six new Cd(II) complexes from 0D to 3D, the reaction routes of **1**–**5'** are shown in Scheme 2. (1) **4**→**3**:. The only N atom from 1,2,4–triazole displays the monodentate mode to connect metal center Cd results in forming the monomer structure of **4**. The effect of aromatic polycarboxylate coligands with different constructions, and multifarious coordination modes on the resultant different structures and topologies cannot be neglected. In order to design and synthesis of high dimensional complexes, The aromatic polycarboxylate auxiliary ligands are key factors to control the connectivity of multidimensional net because they have more coordination sites.[33] Therefore, based on the synthetic procedure of **4**, we introduced auxiliary ligand 1,4–H_2bda and obtained 1D structure of **3**. (2) **3**→**2**: complexes **2** and **3** were prepared using the same reactants but with different molar ratios ($Cd(NO_3)_2{\cdot}4H_2O$ / TMCB / 1,4–H_2bda ligand ratio is 2:1:1 for complex **2** and 1:1:1 for complex **3**. It is proven that higher metal–ligand ratio is apt to permit to construct of high dimension architectures.[34] (3) **2**→**1**: Unexpectedly, when the NaOH was added in the reaction system, the resultant structures of the complexes altered subsequently.[35] In alkaline conditions, the cyangroup of TMCB undergoes hydrolysis to generate the TMCBA. Not only the nitrogen atom in the 1,2,4–triazole but also the oxygen atoms of carboxylic acid can participate in the coordination, and formed 3D structure, consequently no participation of 1,4–H_2bda ligand. (4) **5**→**5'** (effect of TMCB

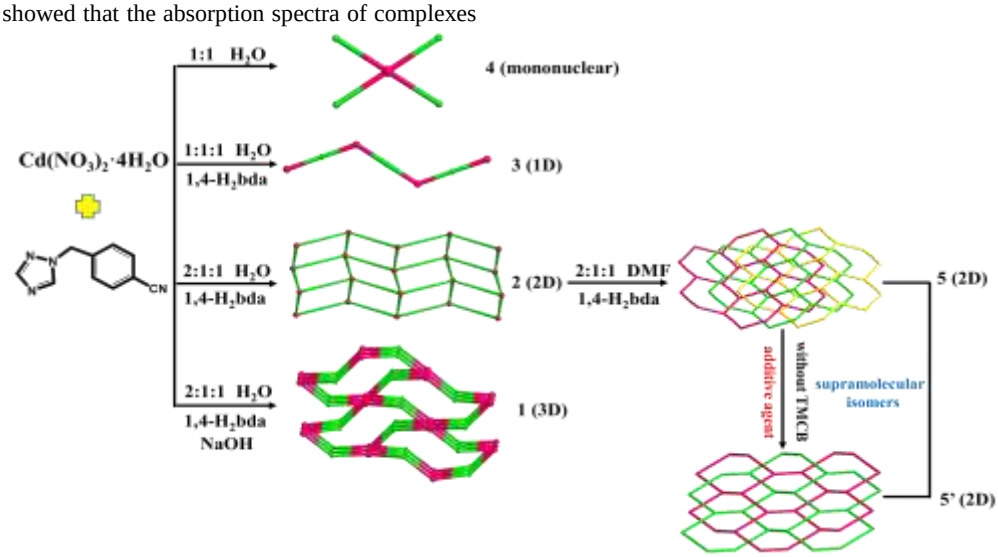

Scheme 2 Reaction routes of complexes **1**–**5'**.

liangd act as additive agents): **5** and **5'** are genuine supramolecular isomers having identical chemical compositions for not only the coordination network but also the whole crystal. So, the formation of supramolecular isomers in this system is dominated by whether the TMCB ligand is used as an additive agent in the reaction.[36-38] In fact, the isomerism arising from the TMCB ligand is fortuitously observed since the additive is not incorporated in the final crystalline product of **5'**. This fact intensively indicates that TMCB molecules may ingeniously influence the micro–environment of the reaction system, generating different superstructures from those crystallized in the absence of TMCB molecules.

Structure Description: {[Cd(TMCBA)$_2$]}$_n$ (1). Single–crystal X–ray diffraction analysis of complex **1** reveals that it contains one Cd^{2+} cation and two crystallographically independent $TMCBA^-$ anions in the asymmetric unit (Fig. S1a). In **1**, the metal center Cd1 is six–coordinated, forming a slightly distorted octahedron with [CdO_4N_2] coordination mode (Fig. S1b). The two carboxylate groups from the $TMCBA^-$ anion provide four bidentate coordination mode μ_2–$\eta_O{}^1$:$\eta_O{}^1$ donor oxygen atoms (O1, O2, O1A and O2A**)** (Scheme S1), and the two triazole rings provide two nitrogen atoms (N1, N1A), respectively. Two adjacent cadmium ions are connected through O1, O2, O1A and O2A atoms deriving from two $TMCBA^-$ anions, giving rise to an infinite 1D linear chain along the *b* axis (Fig. 1a). Along the crystallographic *c* axis, Cd(II) ions are connected by two $TMCBA^-$ ligands (Fig. 1b) to form a 1D "wave–like" chain in which all the metal atoms are coplanar. Two adjacent 1D chains are interconnected to form the 2D layer (Fig. 1c). These 2D layers are further connected into a 3D chair–shaped framework structure (Fig. 2a). In order to simplify the intricate structure of **1**, the secondary building unit (SBUs) [CdO4N2] unit can be considered as a 6–connected node, and $TMCBA^-$ anions could be considered as a 3-connected node (Fig. 2b). The framework exhibits octatomic ring chair–shaped cavity with a size of ca. 20.473 × 10.236 Å (Fig. 2c) according to the Cd1···Cd1 distances. Therefore, the 3D framework of **1** can be described as a rare octatomic ring chair–shaped (3,6)-connected network (Fig. 2d).

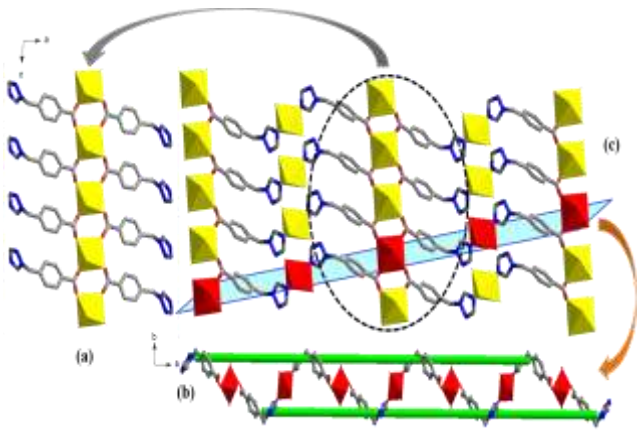

Fig. 1 (a) Polyhedral and ball–and–stick representation of the 1D chain structure along *b* axis in **1**. (b) Polyhedral and ball–and–stick representation of the 1D "wave-like" chain along *c* axis. (c) Polyhedral and ball–and–stick representation of the 2D layer in **1**, hydrogen atoms are omitted for clarity.

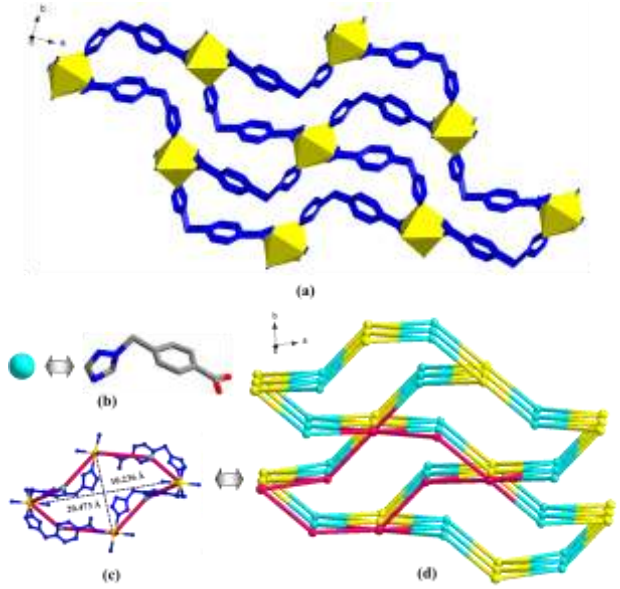

Fig. 2 (a) Polyhedral and ball–and–stick representation of the 3D framework structure in **1**. (b) Blue ball representation of $TMCBA^-$ anion; (c) The detail of the cavities in **1**. (d) Schematic representation of the octatomic ring chair–shaped 3D (3,6)-connected topology in the complex **1**.

[Cd(TMCB)(1,4–bda)(H$_2$O)]$_n$ (2). The asymmetric unit of complex **2** consists of one crystallographically independent Cd^{2+} cations, two TMCB ligands, one 1,4–bda^{2-} anion, and one coordinated water molecule (Fig. S2a). Every Cd^{2+} cation is seven coordinated with slightly distorted pentagonal bipyramid coordination geometry [CdO_5N_2] by four O atoms (O1, O2, O4 and O5) from 1,4–bda^{2-} adopting bidentate-chelate μ_2= η^1:η^1:η^1:η^1 bridging fashion (Scheme S2), one O3 from one coordination water molecule, and two nitrogen atoms (N1 and N2) from TMCB ligand (Fig. S2b). The adjacent cadmium ions are interconnected through O1, O2, O4 and O5 atoms along the *a* axis, formed an infinite 1D "wave–like" chain (Fig. 3a). Each TMCB ligand links two adjacent cadmium ions with two triazole group nitrogen atoms to form a 1D linear chain structure along the *b* axis (Fig. 3b). Two adjacent chains are interconnected to construct a 2D grid layer (Fig. 3c). From the topological point of view, the Cd^{2+} could be considered as the node, TMCB and 1,4–H_2bda ligands as the linkers. Thus, the 2D framework of **2** can be described as a 4–connected 4^4 net (Fig. S3a). The 3D architecture of **2** is reinforced by the intermolecular hydrogen bonds interaction from O3-H3B···N4 and O3-H3C···O5 (Fig. S3b).

{[Cd$_2$(TMCB)$_4$(1,4–bda)$_2$(H$_2$O)$_2$]$_n$·3H$_2$O}$_n$ (3). It contains two Cd^{2+} cations, four TMCB ligands, two 1,4–bda^{2-} anions, two coordination water molecules and three free water molecules in the asymmetric unit of complex **3** (Fig. S4a). Two Cd^{2+} cations exhibit identical slightly distorted pentagonal bipyramid coordination environments (Fig. S4b). Two 1,4–bda^{2-} anions display the bidentate-chelate μ_2= η^1:η^1:η^1:η^1 mode to connect center metal (Scheme S2). Each Cd^{2+} cation linked with two TMCB ligands into a dimer which is further bridged by 1,4–bda^{2-} anion to form an infinite 1D chain structure (Fig. 4a). Moreover, the chains are linked through O1W-H1WC···O8 hydrogen bonding interactions giving rise to layer (Fig. 4b).

These layers structure are further stabilized by π−π stacking interactions (3.534 Å) between the benzene rings of the two TMCB ligands (Fig. 4c), forming a 3D supramolecular framework (Fig. 4d).

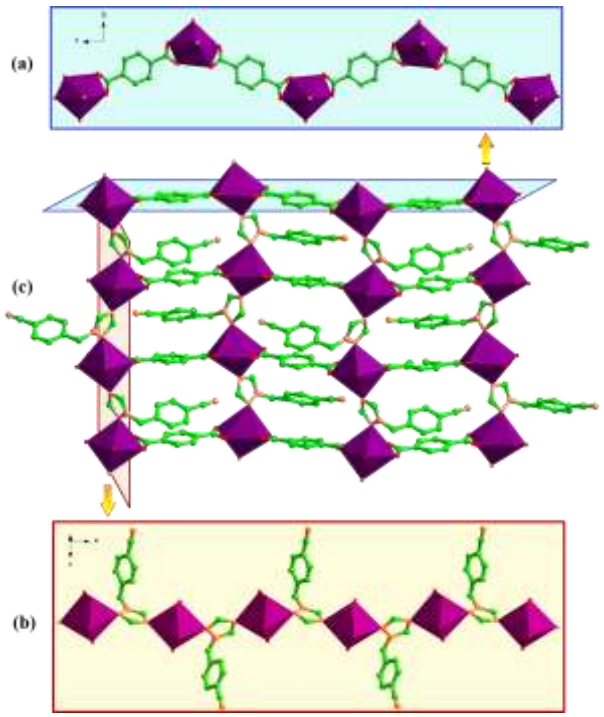

Fig. 3 (a) Polyhedral and ball–and–stick representation of the 1D "wave–like" chain structure along *a* axis in **2**. (b) Polyhedral and ball–and–stick representation of the 1D linear chain structure along *b* axis in **2**. (c) Polyhedral and ball–and–stick representation of the 2D layer in **2** (hydrogen atoms are omitted for clarity).

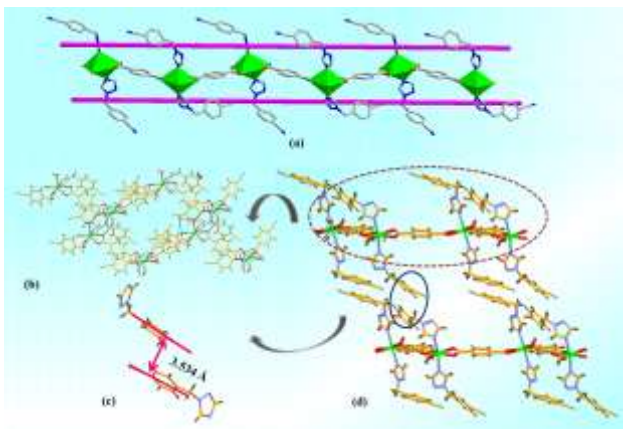

Fig. 4 (a) Polyhedral and ball–and–stick representation of the 1D chain structure in **3** (water molecules and hydrogen atoms are omitted for clarity). (b) The hydrogen bonding interactions between the molecules and (c) packing structure for **3**. (d) A 3D supramolecular structure of **3** (hydrogen bonding is turquoise dashed line).

$\{[Cd(TMCB)_4(H_2O)_2]\cdot(NO_3)_2\cdot(H_2O)_2\}_n$ (4). Complex **4** consists of one Cd^{2+} cation, four crystallographically independent TMCB ligands, two coordinated water molecules, two free water molecules and two free nitrate ions in the asymmetric unit (Fig. S5a). The Cd1 center adopts a distorted octahedral geometry, with four nitrogen atoms from TMCB and two oxygen atoms from coordinated water molecules (Fig. S5b). Each Cd^{2+} cation links four TMCB ligands and two coordinated water molecules to form a mononuclear structure (Fig. 5a). What's more, the triazole ring and benzene ring of each one TMCB ligand are not coplanar. This conformation is further stabilized by intramolecular/intermolecular O–H···O hydrogen bonding, and generated a 3D structure of complex **4** (Fig. 5b).

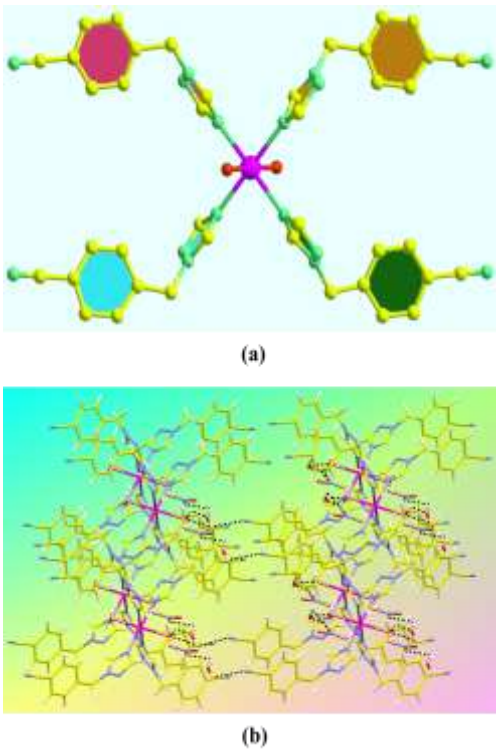

Fig. 5 (a) The illustration of mononuclear structure in **4** (nitrate ions, water molecules and hydrogen atoms are omitted for clarity). (b) The 3D supramolecular structure in **4** (hydrogen bonds are shown by black dots).

$[Cd_{1.5}(1,4–bda)_{1.5}(DMF)_2]_{2n}$ (5). The crystal structure determination reveals that complex **5** contains three crystallographically unique Cd^{2+} cations, three 1,4–bda^{2-} anions, and four DMF molecules, among them, Cd3, Cd4 cations occupies half position (Fig. S6a). Three Cd cations display distorted [CdO_6] octahedral geometry (Fig. S6b). The central Cd3/Cd4 cation is linked to two symmetry–related terminal Cd2 and Cd2A (Cd1 and Cd1A) cations by six carboxylate groups of 1,4–bda^{2-} anions in μ_4–$\eta_O{}^1$:$\eta_O{}^2$:$\eta_O{}^1$:$\eta_O{}^2$ and μ_4–$\eta_O{}^1$:$\eta_O{}^1$:$\eta_O{}^1$:$\eta_O{}^1$ coordination modes (Scheme S2) to afford a Cd_{oct}–Cd_{oct}–Cd_{oct} SBUs with Cd3···Cd2 (Cd3···Cd2A) distance of 3.661(10) Å and Cd4···Cd1 (Cd4···Cd1A) distance of 3.663 (10) Å. Through O9, O9A, O10 and O10A atoms of 1,4–bda^{2-} anion, the linear trinuclear units ($Cd1_{oct}$–$Cd4_{oct}$–$Cd1A_{oct}$) are interconnected to form an infinite 1D "zigzag–like" chain (Fig. 6a). Another "zigzag–like" chain composed of the linear trinuclear units ($Cd2_{oct}$–$Cd3_{oct}$–$Cd2A_{oct}$) is connected with O11, O11A, O12 and O12A atoms originating from the other 1,4–bda^{2-} anion. Furthermore, the two "zigzag–like" chain are further connected by the rest of two 1,4–bda^{2-}

anions to generate the 2D layer structure. Interestingly, in this 2D structure, each central linear trinuclear unit is connected with surrounding six linear trinuclear units through three 1,4–bda^{2-} anions (Fig. 6b). Notably, in a single six membered rings has a channel, which allows the other two identical six membered rings to penetrate, affords a threefold interpenetrating architecture (Fig. 6c).

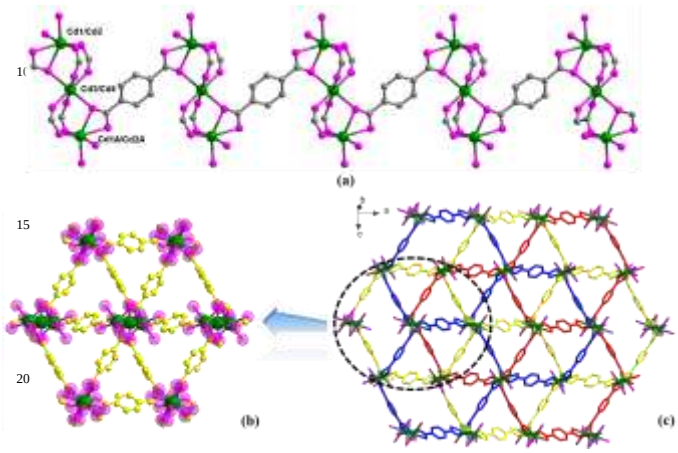

Fig. 6 (a) The 1D "zigzag–like" chain of complex **5** (DMF molecules, water molecules and hydrogen atoms are omitted for clarity). (b) The illustration of single 2D layer in **5**. (c) A threefold interpenetration 2D honeycomb 3-connected layer of **5**.

If the symmetrical trinuclear unit can be regarded as a 3–connected node, connected with three 1,4–bda^{2-} anions. In turn, the 1,4–bda^{2-} anions can be considered as linear bridges between two nodes, the structure of **5** can reduced to a threefold interpenetration 2D honeycomb 3-connected network (Fig. S7a). It is worth noting that there are intermolecular forces between the adjacent the 2D threefold interpenetration layers to form a 3D structure (Fig. S7b).

$[Cd_{1.5}(1,4–bda)_{1.5}(DMF)_2]_{2n}$ (5'). The supramolecular isomeric 2D network of **5'** was obtained under similar reaction conditions without TMCB ligand as an additive agent. Structural analysis indicates that asymmetric unit of **5'** consists of completely identical components to those in **5 (**Fig. S8a). In contrast to **5**, the terminal Cd1 and Cd1A cations exhibit [CdO_7] distorted pentagonal bipyramid geometry. The middle Cd2 cation displays distorted octahedral geometry with [CdO_6] **(**Fig. S8b). The three 1,4–bda^{2-} anions with μ_4–η_O^1:η_O^2:η_O^1:η_O^1 and μ_4–η_O^1:η_O^2:η_O^1:η_O^2 mode bind three Cd(II) centers (Scheme S2). Cd1 and Cd1A are linked to Cd2 via carboxylate groups, forming a trinuclear Cd_{penta}–Cd_{oct}–Cd_{penta} SBUs. The carboxylate groups of the 1,4–bda^{2-} anions link the trinuclear SBUs into an infinite 1D "wave–like" chain (Fig. 7a), which contains a Cd···Cd separation of 3.659(10) Å. Such 1D "wave–like" chains are further interconnected by each other, leading to the formation of a 2D layer structure along the *a* axis (Fig. 7b). Notably, two 2D layers are interpenetrating with each other to give a double–layered motif. It's clear that the double–layers formed twofold interpenetration structure along the *c* axis (Fig. 7c).

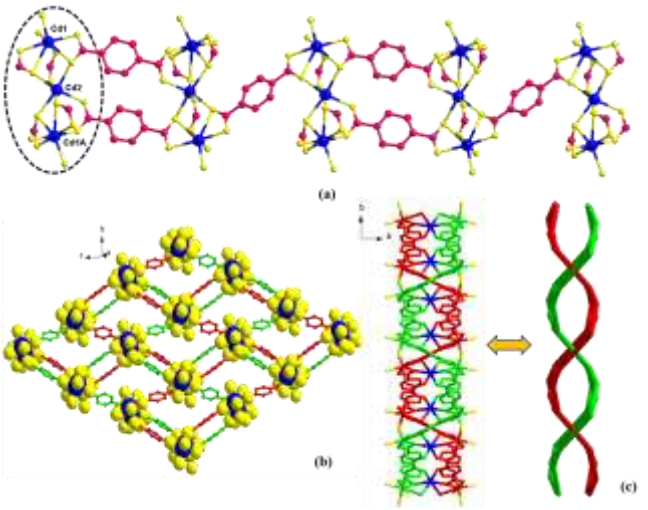

Fig. 7 (a) The 1D "wave–like" chain of complex **5'** (DMF molecules, water molecules and hydrogen atoms are omitted for clarity). (b) The illustration of 2D layer in **5** along *a* axis. (c) A twofold interpenetration 2D honeycomb 3-connected layer of **5'** along *c* axis.

From a topological perspective, the whole framework of **5'** can be topologically represented as twofold interpenetration 2D honeycomb 3-connected network (Fig. S9a), which are further stacked up by intermolecular forces to complete the final 3D structure (Fig. S9b).

To check the phase purity of the products, powder X–ray diffraction (PXRD) experiments have been carried out for complexes **1**–**5'** (Fig. S10). The peak positions of the experimental and simulated PXRD patterns are in good agreement with each other, indicating that the crystal structures are truly representative of the bulk crystal products.[39] The differences in intensity may be owing to the preferred orientation of the crystal samples. Variable–temperature X–ray powder diffraction (VT–XRPD) patterns were obtained using a PANalytical X–ray diffractometer, equipped with monochromated Cu Kα radiation 40 mA, 40 kV. Each powder pattern was recorded in the 5–50 °C range (2θ) from 50 °C to 700 °C with a step of 0.02° and a counting time of 0.4 s. The temperature ramp between two consecutive temperatures was 10 °C/min (Fig. S11). The results confirm that for **1**, no framework change occurs before 250 °C. The diffraction signature might reflect that the network starts to undergo a phase transition from 300 to 400 °C, which induces the structure collapse. After the structure destruction, only 10.9° and 28.2° (2θ) peak is visible, which induces the structure collapse to CdO. The X–ray thermodiffractogram of **1** is consistent well with the TG analyses. [40-42]

Thermal analysis complexes 1–5'. Thermogravimetric experiments were conducted to study the thermal stability of complexes **1**–**5'** (Fig. S12). In the TGA curve of **1**, there is one continuous weight–loss step. The weight loss of 72.15% in the temperature range of 368~492 °C corresponds to two $TMCBA^-$ anoins which is in accordance with the calculated value of 78.25%. The TGA curve shows that **2** has three weight–loss stages. The first weight–loss of 3.80% in the temperature range of 62~90 °C is attributed to the loss of one coordination water molecule. The

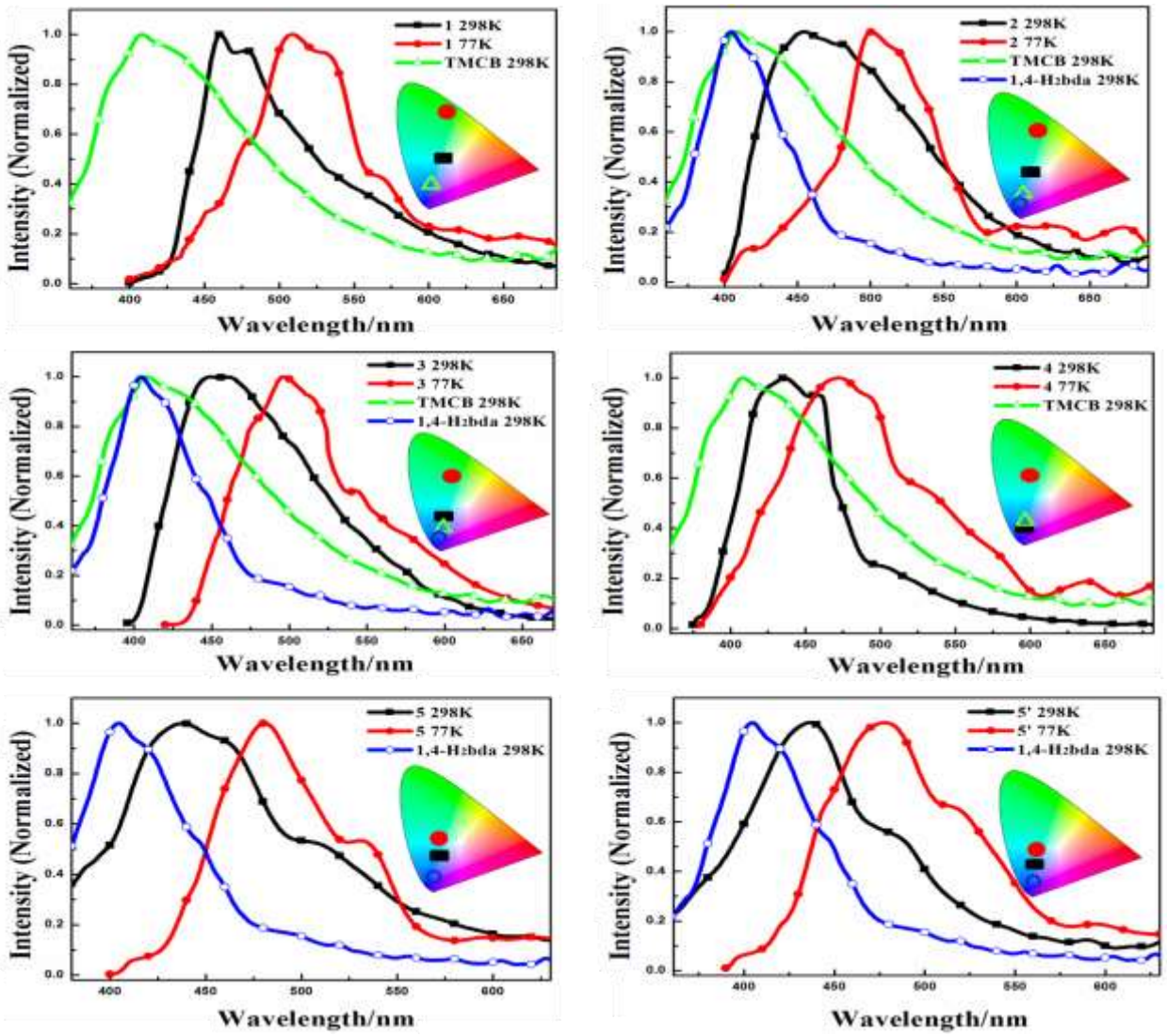

Fig. 8 Normalized emission spectra of complexes **1–5'** at 298 K, 77 K, and TMCB, 1,4–H_2bda at 298 K in solid state and the corresponding color coordinate diagram of emission.

value is close to the calculated value of 3.76%. The loss of 35.12% occurring at the second step is attributed to one 1,4–bda^{2-} anion in the range of 160–252 °C (calcd: 34.28%). The third weight–loss of 40.06% at 252–360 °C is considered as the one TMCB ligand (calcd: 38.48%). Then the TGA of **3** shows three step weight–loss process, the first weight–loss of 6.34% in the temperature range of 276–295 °C, and the following weight–loss of 23.34% during 300–390 °C, which corresponds to the set free of two coordination water molecules, three free water molecules (calcd: 6.53%) and the two 1,4–bda^{2-} anions (calcd: 23.79%), respectively. The third step loses weight from 400 °C to 500 °C corresponding to the loss of four TMCB ligands (obsd: 54.26%, calcd: 53.39%). For **4**, the first weight loss from 240 °C to 316 °C is attributed to the release of two coordinated water molecules, two free water molecules and two free nitrate ions (obsd: 12.45%; calcd: 12.82%). The second weight loss of 71.15% (calcd: 70.49%) from 390 °C corresponds to the loss of four TMCB ligands. **5** and **5'** are supramolecular isomers, therefore, the thermal behaviors of **5** and **5'** display two similar weight loss steps. The first of 26.85% from 200 °C to 380 °C, is assigned to the loss of four DMF molecules (calcd: 26.06%). The second weight loss of 44.21% from 380 °C to 490 °C corresponds to the decomposition three 1,4–bda^{2-} anions.[43] **1** and **4** possess high thermal stability, which deserves to be explored for the application in DSSCs.

Luminescence properties: Inorganic−organic hybrid coordination complexes, especially with d^{10} metal centers, have been investigated for luminescence properties owing to their potential applications as luminescent materials.[44] The emission spectrum of solid–state sample (Fig. 8) of **1** is centered at 461 nm (455 nm for **2**, 449 nm for **3**, 436 nm for **4**, 438 nm for **5**, 433 nm for **5'**, 408 nm for TMCB and 405 nm for 1,4–H_2bda), exhibiting deep blue, blue and light blue luminescent emissions with CIE (Commission Internacionale d'Eclairage) coordinates of **1–5'** at 298 K (Fig. 8). These luminescent emissions may be attributed to the ligand-centered $\pi^* \rightarrow \pi$ transition (Scheme 3).[45] However, the role of structural complexity and framework

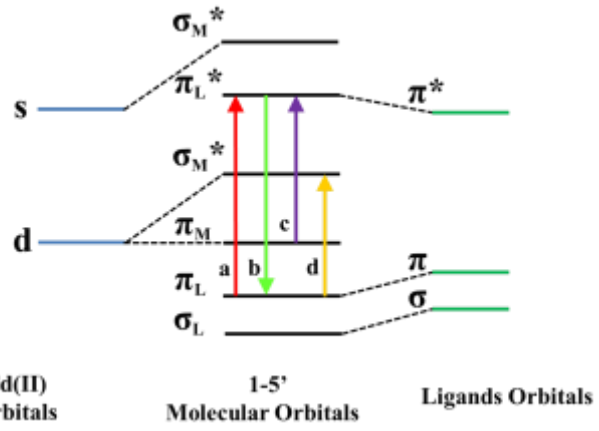

Scheme 3 Schematic energy level diagram of complexes **1–5'** molecular orbitals (a, π→π*; b, π*→π; c, MLCT; d, LMCT).

robustness cannot be ignored. Considering the above factors, it is equally difficult to assign its emissions, as it is neither metal–to–ligand charge transfer (MLCT) nor ligand–to–metal charge transfer (LMCT) (Scheme 3).

The solid state luminescence spectra of **1–5'** at liquid nitrogen temperature are researched. At 77 K, **1–5'** emits intensely at 509 nm, 501 nm, 496 nm, 472 nm, 481 nm and 478 nm, which are at the deep green and green (Fig. 8). The change of temperature from 298 K to 77 K caused a bathochromic shift of emission peaks in solid state of **1–5'**. The shift in luminescence spectra at low temperatures so called "luminescence thermochromism" is usually explained by predomination "cluster centred".[46] There are more free water molecules in **3** than that in **2**, which can increase the radiationless transition and cause blue shift for the maximum emission. Besides that, we can conclude that the shift of the maximum emission in **1−5'** may be attributed to the rigidity of complexes **1−5'**. This rigidity is favor of energy transfer and reduces the loss of energy through a radiationless pathway. The possible explanation for the difference emission properties of **1−5'** is the different dimensionality in **1−5'**.

We also performed time–resolved measurements by using the time–correlated single photon counting (TCSPC) technique. The luminescent lifetimes of **1–5'** increase to those at 298 K (298 K: τ = 9.53 μs, 11.17 μs, 12.26 μs, 9.66 μs, 9.83 μs, 12.48 μs for **1–5'**; 77 K: τ = 18.04 μs, 16.63 μs, 18.22 μs, 11.87 μs, 18.23 μs, 16.16 μs for **1–5'**) (Fig. S13), since cold conditions would be favorable to the rigidity of ligands with reducing the non–radiation decay and collisional quenching.[47]

For **1-5'**, we have further examined the effects of solvent polarity on the UV absorption at 298 K, the emission sensitivity, luminescent lifetimes and the quantum yields (Φ) at 298 K and 77K (Fig. S14–Fig.S18), corresponding data are listed in Table S1. In the UV spectra, the electronic absorption spectra of **1–5'** are similar to that of free ligands, which is attributed to the metal perturbed intraligand π→π* transition (Scheme 3).[48] Among them, **1** and **4** have strong absorption in the low wavelength region of ultraviolet and blue-violet. Complexes **1–5'** in different dilute solutions display deep blue, blue and light blue luminescence emissions with CIE coordinates, which are affected by the solvent and temperature. The ^{1}H NMR data indicates that **1–5'** still keeps polymeric structure in solutions and don't decompose.

Application in DSSCs: Encouraged by the UV absorption in three solutions results, complexes **1** and **4** can be considered as co-sensitizers used in N719 sensitized DSSCs. The absorption spectra of the prepared complexes **1**, **4** and N719 in ethanol solutions are shown in Fig. S19, and the corresponding data are listed in Table 1. The electronic absorption spectra of **1** and **4** exhibit two energy absorption bands: two higher energy absorption bands at 331 nm and 324 nm, two low energy absorption bands at 378 nm and 365 nm. Compared with the absorption spectra of N719, apparently, the absorption spectra of **1** and **4** could compensate for that of N719 in the low wavelength region of ultraviolet and blue-violet.

As shown in Table 1, the UV absorption (λ_{max}) appears at 378 nm for **1** and 365 nm for **4**. The molar extinction coefficients in the blue-violet region are 47,016 M^{-1} cm^{-1} for **1** and 45,123 M^{-1} cm^{-1} for **4**. All of these are much higher than that of the ruthenium complex N719.[49] A higher molar extinction coefficient indicates that the **1** and **4** possess a higher light harvesting ability in this wavelength region compared with N719 and I_3^- (25,000M^{-1} cm^{-1}).[50] Hence it can be predicted that the photon lost due to the light absorption by I_3^- will be suppressed by the use of **1** or **4** as a co-sensitizer and co-adsorbent due to the competition between **1** or **4** and I_3^- to absorb light.

On the other hand, energy–level matching is crucial in selecting sensitizer. In order to estimate the HOMO and LUMO energy levels of **1** and **4**, cyclic voltammetry (CV) was carried out in a three–electrode cell and an electrochemistry workstation (Fig. S20). The experimental data for electrochemical properties of complexes are summarized in Table 1. As estimated from the intersection of the absorption and emission spectra, the excitation transition energy (E_{0-0}) of **1** and **4** are 3.10 and 3.15 eV, respectively. Consequently, the HOMO values of **1** and **4** are calculated based on their first redox potentials as –5.32 and –5.41 eV, respectively, and the LUMO levels of **1** and **4** calculated from E_{HOMO} + E_{0-0}, are –2.22 and –2.26 eV, respectively.[51] The HOMO and LUMO energy levels of **1** and **4** are shown in Scheme 4. It shows that the energy levels of **1** and **4** are appropriate for the DSSCs system containing TiO_2. The LUMO levels lied above the conduction band (CB) of the TiO_2 semiconductor (-4.40 eV vs vacuum), indicating efficient electron injection, and the HOMO energy levels lied below the I^-/I_3^- redox electrolyte (-4.60 eV vs vacuum) which is further improved negatively about 0.3 V by adding additives such as 4-tert-butyl pyridine (TBP) to the I^-/I_3^- redox electrolyte,[52] providing sufficient driving force for dye regeneration.[53]

Therefore, complexes **1** and **4** were employed as co–sensitizers and co–adsorbents to fabricate complex/N719 photoanodes. The current–voltage (*J–V*) characteristic of the DSSCs devices based on N719, **1**, **4**, **1**/N719 and **4**/N719 photoanodes are shown in Fig. 9, and the corresponding cells performance are summarized in Table 2. The values of J_{sc} is

Table 1 Experimental data for spectral and electrochemical properties of the complexes **1** and **4**

Dyes	λ_{abs}(nm)[a]	$\varepsilon(M^{-1}cm^{-1})$[a]	λ_{em}(nm)[a,b]	E_{0-0}(eV)[c]	E_{ox}/V vs SCE[d]	E_{HOMO}(eV)[e]	E_{LUMO}(eV)[e]
1	378	47016	414	3.10	0.92	–5.32	–2.22
4	365	45123	395	3.15	1.01	–5.41	–2.26

[a] Absorption and emission spectra were recorded in ethanol solution (10^{-5} M) at room temperature.
[b] Complexes were excited at their absorption maximum value
[c] Optical band gap calculated from intersection between the absorption and emission spectra.
[d] The first oxidation potentials of complexes were obtained by CV measurement.
[e] The values of E_{HOMO} and E_{LUMO} were calculated with the following formula:

$$HOMO\ (eV) = -e(E^{ox}_{onset}\,V + 4.4V);\quad LUMO\ (eV) = E_{HOMO} + E_{0\text{-}0}$$

where E_{0-0} is the intersection of absorption and emission of the complexes **1** and **4**.

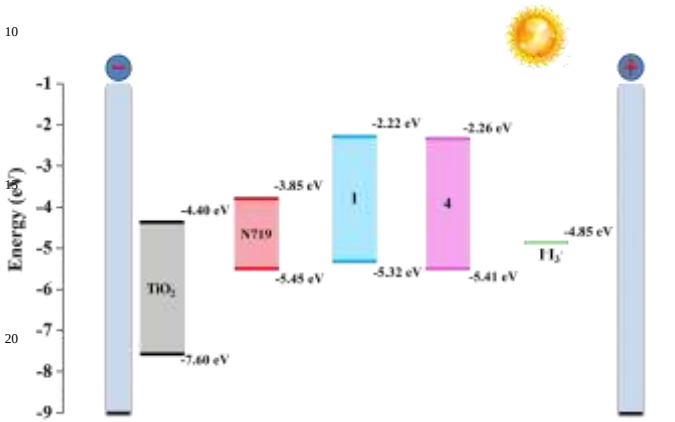

Scheme 4 Schematic energy diagram of HOMO and LUMO for dyes compared to the energy levels calculated for TiO_2.

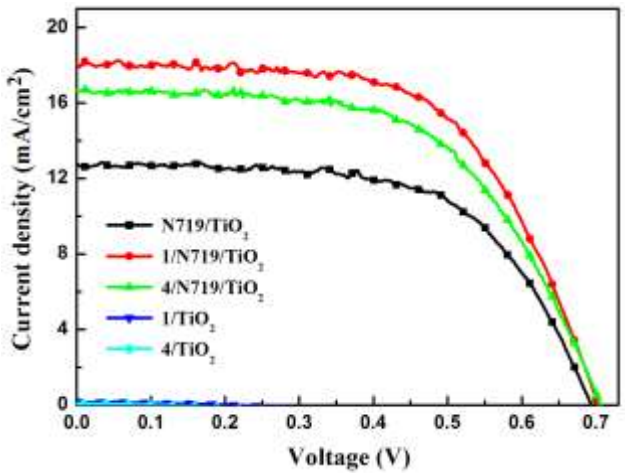

Fig. 9 *J–V* curves for DSSCs based on co–sensitized photoelectrodes and N719, **1**, **4** sensitized photoelectrode under irradiation.

improved in the order of **1**/N719 > **4**/N719 > N719 > **1** > **4** respectively. The **1**/N719 and **4**/N719 device yield J_{sc} of 17.99 mA cm^{-2} and 16.69 mA cm^{-2}, V_{oc} of 0.70 V and 0.71 V, fill factor (*FF*) of 0.61 and 0.58, η of 7.68% and 6.85%. The parameter of η is 40.40% and 25.23% higher than that of the device only sensitized by N719. However, the individually **1** and **4** sensitized devices were found to exhibit a low η value of 0.02% and 0.01%, J_{sc} of 0.14 mA cm^{-2} and 0.12 mA cm^{-2}, V_{oc} of 0.28 V and 0.25 V, *FF* of 0.40 and 0.37.

Table 2 *J–V* performance of DSSCs based on different photoelectrodes

Photoelectrode	J_{sc}/mA/cm^2	V_{oc}/V	*FF*	η/%
1/TiO_2	0.14	0.28	0.40	0.02
4/TiO_2	0.12	0.25	0.37	0.01
N719/TiO_2	12.78	0.69	0.62	5.47
1/N719/TiO_2	17.99	0.70	0.61	7.68
4/N719/TiO_2	16.69	0.71	0.58	6.85

The enhanced J_{sc} value is ascribed to the enhanced IPCE response of the cell, since they are related by the equation:

$$J_{sc} = \int e\phi_{\text{ph.AM1.5G}}(\lambda)d\lambda$$

where e is the elementary charge and ϕ ph.AM1.5G is the photon flux at AM 1.5.[54] The IPCE spectra of different devices were collected in Fig. 10. The DSSCs containing only N719 dye has a broad IPCE spectrum from 300-750 nm but a decrease in the wavelength range of 340-450 nm, which is due to the competitive light absorption between I_3^- and N719. When

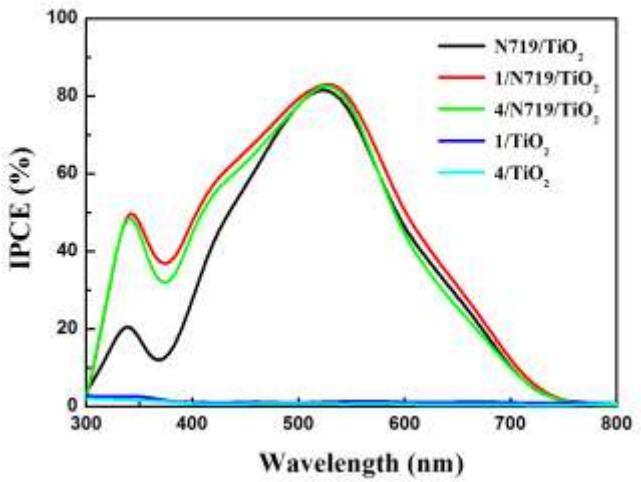

Fig. 10 The incident photon-to-current conversion efficiency spectra of devices based on single N719, **1**, **4** sensitized and co-sensitized photoanodes.

the prepared complexes are used as co-sensitizer, this decrease is restored a lot. This means the co-sensitization of N719 and prepared complexes has a significant synergy and compensatory effect on light harvesting, electron injection and collection on TiO_2. Based on the IPCE and the absorption spectra, the cell's higher J_{sc} in the case of co-sensitization is mainly ascribed to better light harvesting in the low wavelength region, where the absorption of N719 is compensated and the competitive light absorption of

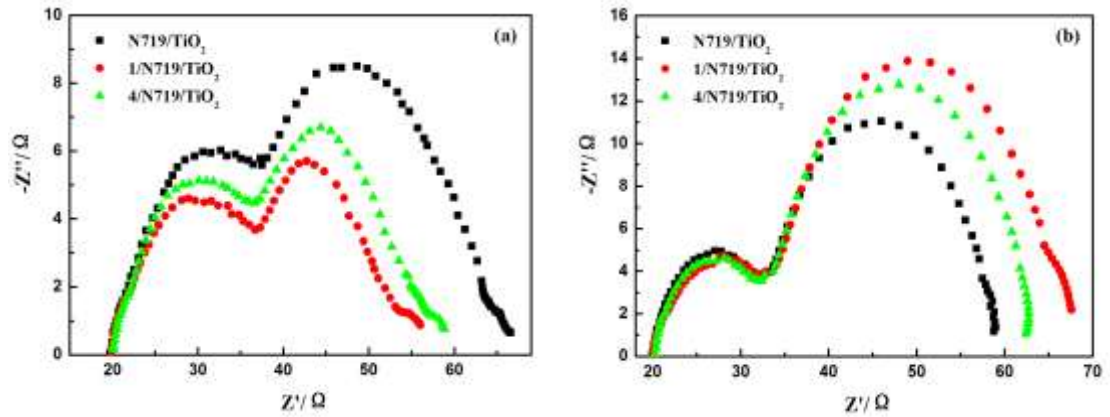

Fig. 11 Nyquist plots of EIS for DSSCs based on different photoelectrodes measured under standard AM1.5 G solar irradiation (a) and in dark (b) at forward bias –0.75V.

I_3^- is overcome. On the other hand, the bad IPCE response of **1** and **4** individually sensitized DSSC is the reason of its low J_{sc}. And the J_{sc} in co-sensitized devices is not a result of summation. However, this confirms that there is a significant synergy and compensatory effect between **1** or **4** and N719.

We utilized electrochemical impedance spectroscopy (EIS) to analyze charge carrier dynamics in the interfacial regions of solid–liquid layers. Usually, in DSSCs system, each EIS curve contains three semicircles that are representative for the resistance states of different interfaces.[55] The three semicircles located in high, middle and low frequency regions (left to right) are attributed to the electrochemical reaction at the Pt/electrolyte interface, the charge transfer at the TiO_2/dye/electrolyte interface and a Warburg diffusion process of the I^-/I_3^- in the electrolyte.[56]

Under light illumination, EIS was utilized to analyze the charge transport resistance at the TiO_2/dye/electrolyte interface for its significance on the efficiency of DSSCs. As shown in Fig. 11a, The radius of the large semicircle located in middle frequency regions in the Nyquist plots decrease after co–sensitized with complexes, and the values are in sequence for **1**/N719 < **4**/N719 < N719, which indicates a decrease of the electron transfer impedance and an increase of charge transfer rate at this interface after co–sensitization. while in the dark, this semicircle radius in the Nyquist plot increased after co-sensitized with complexes, and the values are in the order of **1**/N719 > **4**/N719 > N719, which indicates an increase of electron recombination impedance and a reduction of the interfacial charge recombination rate (Fig. 11b). Higher charge transfer rate and lower charge recombination rate are benefit for enhancing performance of DSSCs.

For complex **1**, it adsorbed on Nano TiO_2 thin film surface through carboxyl which has various coordination modes with metal ions, such as bidentate-monatomic, chelate-monatomic, *etc*. Although carboxyl has coordinated to the Cd^{2+} ion in complex **1**, Ti^{4+} ion may also be coordinated with carboxyl due to the existence of lone pair electrons in carboxylate oxygen atom which could combine with Ti^{4+} ion to form Ti-O coordination bond, and further adsorbed on the TiO_2 film. While for complex **4**, the nitrogen atoms of 1,2,4-triazole were expected to adsorb at the Lewis acid sites of the TiO_2 surface as the nitrogen atom in pyridine.[57] While, adsorption on Nano TiO_2 surface through carboxyl, making its excited electron easily injected into the conduction band of Nano TiO_2. This is the reason why complex **1** obtained a higher efficiency than complex **4** when they were co-sensitized with N719, respectively.

Conclusion

In conclusion, six new complexes have been successfully synthesized through the hydro(solvo)thermal reactions of Cd(II) salts with the new multifunctional ligand TMCB. Through controlling the reaction conditions, TMCBA was obtained from the cyanophoric hydrolytic reaction. Complexes **1**–**5'** exhibited mononuclear, 1D, 2D and 3D architectures, respectively. The structural diversities of the complexes indicate that the TMCB ligand is good candidates for the construction of complexes with fascinating motifs. The tunable luminescence emissions show that the complexes **1**–**5'** may be good candidates for photoactive materials. It is anticipated that other new complexes with intriguing structures as well as chemical or physical properties may also be synthesized through using the 4-(1,2,4-triazolylmethyl) cyanobenzene ligand. It's worth noting that, complexes **1** and **4** can be applied with N719 in DSSCs as a co-sensitizer, which will enhance the photo-electricity efficiency and improve both J_{sc} and V_{oc}. The co-sensitized devices exhibit an enhanced performance, and both of them are higher than that of single N719 sensitized solar cells. Complexes **1** and **4** co-sensitized device yields the overall efficiency of 7.68% and 6.85%, which is 40.40% and 25.23% greater than that of the device containing only N719 (5.47%). The newly developed co-sensitizer is anticipated to arouse broad interest in further boosting the efficiency of dye sensitized solar cell by a simple sequential adsorption process, which explores a new domain for the use of these type complexes.

Acknowledgements

This work was supported by National Natural Science Foundation of China (Grant 21371040 and 21171044), the

National key Basic Research Program of China (973 Program, No. 2013CB632900), supported by the Fundamental Research Funds for the Central Universities (Grant No. HIT. IBRSEM. A. 201409), and Program for Innovation Research of Science in Harbin Institute of Technology (PIRS of HIT No. A201416 and B201414).

References

1 Z. C. Hu, B. J. Deibert and J. Li, *Chem. Soc. Rev*., 2014, **43**, 5815–5840.
2 J. Heine and K. M. Buschbaum, *Chem. Soc. Rev*., 2013, **42**, 9232–9242.
3 Y. Li, H. Song, Q. Chen, K. Liu, F. Y. Zhao, W. J. Ruan and Z. Chang, *J. Mater. Chem. A.*, 2014, **2**, 9469–9473.
4 M. D. Allendorf, C. A. Bauer, R. K. Bhakta and R. J. T. Houk, *Chem. Soc. Rev*., 2009, **38**, 1330–1352.
5 J. H. Wang, M. Li and D. Li, *Chem. Sci.*, 2013, **4**, 1793–1801.
6 C. Bechinger, S. Ferrere, A. Zaban, J. Sprague and B. A. Gregg, *Nature*, 1996, **383**, 608–610.
7 J. C. Crano, T. Flood, D. Knowles, A. Kumar and B. Van Gemert , *Pure Appl. Chem.*, 1996, **68**, 1395–1398.
8 C. C. Corredor, Z. L. Huang, K. D. Belfield, A. R. Morales and M. V. Bondar, *Chem. Mater*., 2007, **19**, 5165–5173.
9 Y. Yokoyama, *Chem. Rev*., 2000, **100**, 1717–1739.
10 A. Schneemann, V. Bon, I. Schwedler, I. Senkovska, S. Kaskel and R. A. Fischer, *Chem. Soc. Rev*., 2014, **43**, 6062–6096.
11 F. A. Almeida Paz, J. Klinowski, S. M. F. Vilela, J. P. C. Tomé, J. A. S. Cavaleiro and J. Rocha, *Chem. Soc. Rev*., 2012, **41**, 1088–1110.
12 X. J. Yuan, X. X. Zhang, H. Zhao, L. N. Liu and B. L. Wu, *Cryst. Growth Des*., 2013, **13**, 4859−4867.
13 J. S. Qin, S. R. Zhang, D. Y. Du, P. Shen, S. J. Bao, Y. Q. Lan and Z. M. Su, *Chem. Eur. J.*, 2014, **20**, 5625–5630.
14 L. Croitor, E. B. Coropceanu, A. E. Masunov, H. J. Rivera-Jacquez, A. V. Siminel and M. S. Fonari, *J. Phys. Chem. C.*, 2014, **118**, 9217–9227.
15 L. Croitor, E. B. Coropceanu, A. E. Masunov, H. J. Rivera-Jacquez, A. V. Siminel, V. I. Zelentsov, T. Y. Datsko and M. S. Fonari, *Cryst. Growth Des*., 2014, **14**, 3935−3948.
16 H. Wu, X. L. Lü, C. L. Yang, C. X. Dong and M. S. Wu, *CrystEngComm*, 2014, **16**, 992–1000.
17 X. L. Wang, D. Zhao, A. X. Tian and J. Ying, *Dalton Trans*., 2014, **43**, 5211–5220.
18 Y. Yang, P. Du, J. Yang, W. Q. Kan and J. F. Ma, *CrystEngComm*, 2013, **15**, 4357–4371.
19 P. Yang, X. X. Wu, J. Z. Huo, B. Ding, Y. Wang and X. G. Wang, *CrystEngComm*, 2013, **15**, 8097–8109.
20 O. V. Sharga, A. B. Lysenko, M. Handke, H. Krautscheid, E. B. Rusanov, A. N. Chernega, K. W. Krämer, S. X. Liu, S. Decurtins, A. Bridgeman and K. V. Domasevitch, *Inorg. Chem*., 2013, **52**, 8784–8794.
21 Y. H. Luo, F. X. Yue, X. Y. Yu, L. L. Gu, H. Zhang and X. Chen, *CrystEngComm*, 2013, **15**, 8116–8124.
22 N. Wang, Y. C. Feng, W. Shi, B. Zhao, P. Cheng, D. Z. Liao and S. P. Yan, *CrystEngComm*, 2012, **14**, 2769–2778.
23 X. X. Li, H. Y. Xu, F. Z. Kong and R. H. Wang, *Angew. Chem. Int. Ed*., 2013, **52**, 13769–13773.
24 M. Yang, Z. J. OuYang, W. B. Chen, R. F. Zhou, N. Li and W. Dong, *CrystEngComm*, 2013, **15**, 8529–8536.
25 X. Y. Huang, S. Y. Han, W. Huang and X. G. Liu, *Chem. Soc. Rev*., 2013, **42**, 173–201.
26 L. Y. Zhang, Y. L. Yang, R. Q. Fan, P. Wang and L. Li, *Dyes Pigm.*, 2012, **92**, 1314–1319.
27 L. G. Wei, Y. L. Yang, R. Q. Fan, Y. Na, P. Wang, Y. W. Dong, B. Yang and W. W. Cao, *Dalton Trans*., 2014, **43**, 11361–11370.
28 X. Wang, Y. L. Yang, P. Wang, L. Li, R. Q. Fan, W. W. Cao, B. Yang, H. Wang and J. Y. Liu, *Dalton Trans.*, 2012, **41**, 10619–10625.
29 D. D. Wang, Y. Wu, H. Dong, Z. X. Qin, D. Zhao, Y. Yu, G. J. Zhou, B. Jiao, Z. X. Wu, M. Gao and G. Wang, *Org. Electron*., 2013, **14**, 3297–3305.
30 H. Kusama, T. Funaki, N. Koumura and K. Sayama, *Phys. Chem. Chem. Phys*., 2014, **16**, 16166–16175.
31 S. P. Singh, K. S. V. Gupta, M. Chandrasekharam, A. Islam, L. Y. Han, S. Yoshikawa, M. Haga, M. S. Roy and G. D. Sharma, *ACS Appl. Mater. Inter.*, 2013, **5**, 11623–11630.
32 R. Menzel, D. Ogermann, S. Kupfer, D. Weiß, H. Görls, K. Kleinermanns, L. González and R. Beckert, *Dyes Pigm.*, 2012, **94**, 512–524.
33 C. Y. Xu, L. K. Li, Y. P. Wang, Q. Q. Guo, X. J. Wang, H. W. Hou and Y. T. Fan, *Cryst. Growth Des*., 2011, **11**, 4667−4675.
34 R. Q. Fan, L. Y. Wang, P. Wang, H. Chen, C. F. Sun, Y. L. Yang and Q. Su, *J. Solid State Chem.*, 2012, **196**, 332-340.
35 P. Yang, M. S. Wang, J. J. Shen, M. X. Li, Z. X. Wang, M. Shao and X. He, *Dalton Trans*., 2014, **43**, 1460–1470.
36 L. M. Fan, X. T. Zhang, D. C. Li, D. Sun, W. Zhang and J. M. Dou, *CrystEngComm*, 2013, **15**, 349–355.
37 C. P. Li, J. M. Wu and M. Du, *Inorg. Chem*., 2011, **50**, 9284–9289.
38 J. P. Zhang, X. C. Huang and X. M. Chen, *Chem. Soc. Rev*., 2009, **38**, 2385–2396.
39 J. Yang, J. F. Ma, Y. Y. Liu and S. R. Batten, *CrystEngComm*, 2009, **11**, 151–159.
40 B. Liu, R. L. Zhao, G. P. Yang, L. Hou, Y. Y. Wang and Q. Z. Shi, *CrystEngComm*, 2013, **15**, 2057–2060.
41 C. Volkringer, M. Meddouri, T. Loiseau, N. Guillou, J. Marrot, G. Férey, M. Haouas, F. Taulelle, N. Audebrand and M. Latroche, *Inorg. Chem*., 2008, **47**, 11892–11901.
42 W. Kaneko, M. Ohba and S. Kitagawa, *J. Am. Chem. Soc.* 2007, **129**, 13706–13712.
43 F. Wang, X. M. Jing, B. Zheng, G. H. Li, G. Zeng, Q. S. Huo and Y. L. Liu, *Cryst. Growth Des*., 2013, **13**, 3522−3527.
44 C. A. Bauer, T. V. Timofeeva, T. B. Settersten, B. D. Patterson, V. H. Liu, B. A. Simmons and M. D. Allendorf, *J. Am. Chem. Soc.* 2007, **129**, 7136–7144.
45 R. Q. Fan, Y. L. Yang, Y. B. Yin, W. Hasi and Y. Mu, *Inorg. Chem*., 2009, **48**, 6034–6043.
46 I. Jeß, P. Taborsky, J. Pospíšil and C. Näther, *Dalton Trans.*, 2007, 2263-2270.
47 R. R. Hu, C. F. A. Gómez-Durán, J. W. Y. Lam, J. L. Belmonte-Vázquez, C. M. Deng, S. J. Chen, R. Q. Ye, E. Peña-Cabrera, Y. C. Zhong, K. S. Wong and B. Z. Tang, *Chem. Commun*., 2012, **48**, 10099–10101.
48 Y. X. Zhou, X. Q. Shen, C. X. Du, B. L. Wu and H. Y. Zhang, *Eur. J. Inorg .Chem*., 2008, 4280–4289.
49 D. B. Kunag, S. Ito, B. Wenger, C. Klein, J. E. Moser, R. Humphry-Baker, S. M. Zakeeruddin and M. Grätzel, *J. Am. Chem. Soc*., 2006, **128**, 4146–4154.
50 G. D. Sharma, S. P Singh, R. Kurchania and R. J. Ball, *RSC Adv.*, 2013, **3**, 6036–6043.
51 C. M. Cardona, W. Li, A. E. Kaifer, D. Stockdale and G. C. Bazan, *Adv. Mater*., 2011, **23**, 2367–2371.
52 G. Boschloo, L. Ha1ggman and A. Hagfeldt, *J. Phys. Chem. B*, 2006, **110**, 13144–13150.
53 K. R. Justin Thomas, Y. C. Hsu, J. T. Lin, K. M. Lee, K. C. Ho, C. H. Lai, Y. M. Cheng and P. T. Chou, *Chem. Mater.*, 2008, **20**, 1830–1840.
54 A. Hagfeldt, G. Boschloo, L. C. Sun, L. Kloo and H. Pettersson, *Chem. Rev*., 2010, **110**, 6595–6663.
55 J. Bisquert, A. Zaban, M. Greenshtein and I. Mora-Sero, *J. Am. Chem. Soc*., 2004, **126**, 13550–13559.
56 D. Kuang, S. Uchida, R. Humphry-Baker, S. M. Zakeeruddin and M. Grätzel, *Angew. Chem. Int. Ed*., 2008, **47**, 1923–1927.
57 Y. Harima, T. Fujita, Y. Kano, I. Imae, K. Komaguchi, Y. Ooyama and J. Ohshita, *J. Phys. Chem. C.*, 2013, **117**, 16364–16370.

Table of Content

Application in dye–sensitized solar cells and luminescence properties: an insight into the controllable synthesis of Cd(II) complexes with the new multifunctional ligand

Song Gao,[a] Rui Qing Fan,*[,a] Xin Ming Wang,[a] Liang Sheng Qiang,[a] Li Guo Wei,[a] Ping Wang,[a] Hui Jie Zhang,[a] Yu Lin Yang*[,a], Yu Lei Wang[b]

[a]*Department of Chemistry, Harbin Institute of Technology, Harbin 150001, P. R. of China*

[b]*National Key Laboratory of Science and Technology on Tunable Laser, Harbin Institute of Technology, Harbin 150080, P. R. of China*

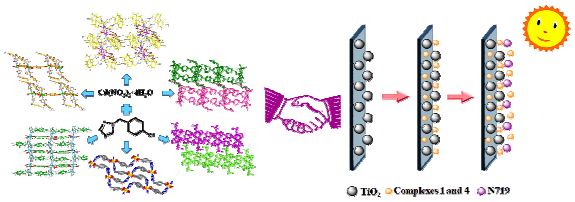

This synergism, resulting from the combination of luminescence and DSSCs, opens up the way to new multifunctional materials.